Alkali etching enhanced polyimide based three-layer composite separator for lithium-ion batteries

Wenzhao Jiang
Guangzhou Nanyang Polytechnic College
Youpeng Chen
Guangdong University of Technology
Jiangyun Zhang
Guangdong University of Technology
Guoqing Zhang
Guangdong University of Technology
Dongqing Cao
Guangdong University of Technology
Xinxi. Li (xinxili168@163.com)
Guangdong University of Technology
Junyuan Liu
Guangdong University of Technology

Research Article

Keywords: Lithium-ion batteries separators, Electrostatic spinning, Non-solvent phase separation, Alkali etching

Posted Date: December 29th, 2023

DOI: https://doi.org/10.21203/rs.3.rs-3789907/v1

Additional Declarations: No competing interests reported.

Abstract

Separators has directly affected the safety and electrochemical performance of lithium-ion batteries. In this study, an alkali etched enhanced polyimide (PI)/polyacrylonitrile (PAN)@ (Cellulose acetate) CA/PI three-layer composite separator is prepared using electrospinning, non-solvent phase separation, and alkali etching methods. The effects of alkali etching on the mechanical strength, thermal stability, and electrochemical performance of the PI/PAN@CA/PI separator are explored. The obtained separator has two different pore structures, and the surface of the alkali etched separator has abundant polar groups, further enhancing the migration rate of lithium-ions. The mechanical strength and thermal performance decrease with the prolongation of alkali etching time. When the alkali etching time is 3 min, the PI/PAN@CA/PI separator has the best comprehensive performance, with a mechanical strength of 17.8 MPa, ion conductivity of 1.22 mS cm^{-1}, and interface impedance of 152 Ω. After 100 cycles of charging and discharging at a current density of 1 C, the capacity retention rate is 95.3%. At a current density of 5 C, the specific capacity of charging and discharging can reach 114 mAh g^{-1}, which is better than the 87.3 mAh g^{-1} of the initial PI/PAN@CA/PI separator.

1. Introduction

At present, lithium-ion batteries are constantly developing towards high energy density. As one of the key components in lithium-ion battery, the separator is responsible for the transmission channel of lithium ion between electrodes, which can prevent short circuits caused by direct contact between positive and negative electrodes[1]. Besides, the separator can directly affect the capacity and safety of lithium-ion batteries during charging and discharging process[2, 3]. Generally, the separator materials are mainly polyolefins, which have some drawbacks such as poor porosity, electrolyte affinity, and thermal stability[4]. It is not satisfied to the requirement of high energy density lithium-ion batteries. Currently, the researchers have made various modifications to the polyolefin separator in various directions such as inorganic ceramic and organic temperature resistant polymer[5, 6]. However, due to the limitation of polyolefin materials, it is very necessary to explore separator with excellent electrochemical performance and thermal stability.

The fiber separator prepared by electrospinning method is widely used in the field of lithium-ion battery separators due to its three-dimensional network structure and high porosity[7]. Common separator materials include polyacrylonitrile (PAN), polyimide (PI), polyvinylidene fluoride (PVDF)[8–11]. PAN fiber separators have been widely studied due to their high electronic insulation, excellent electrolyte affinity, and ion conductivity[12]. However, the low mechanical strength of polyacrylonitrile fiber separators affects their application in lithium-ion batteries[13].

The separator prepared by non-solvent phase separation method has an interconnected porous structure and is commonly used for large-scale preparation of lithium-ion battery separators[14]. By adjusting different coagulation bath solutions or adding different pore forming agents, different pore structures and

pore sizes can be obtained[15–17]. PI non solvent phase separation separator has good mechanical strength, and the connected porous structure can effectively store the electrolyte in the separator[18]. However, the low porosity makes it difficult for non-solvent phase separation separators to demonstrate the excellent energy density of lithium-ion batteries.

In order to prepare separators with better electrochemical performance, it is often necessary to modify them. Common material modification methods include physical blending modification and chemical modification. Cellulose acetate (CA) is an organic ester of cellulose, which is the first commercial variety among cellulose derivatives. Because it contains more ester groups in its chemical chain, has strong electrolyte affinity and excellent chemical stability, it is often used as a physical blending modification material[19, 20]. Alkali etching is a commonly used modification method in chemical modification. Alkali etching reacts with materials to form new chemical bond and improve the electrochemical performance of the separator[21–23].

This study combines the structural advantages of electrospinning and non-solvent phase separation methods to prepare separators, and utilizes physical mixing and chemical modification methods to design an alkali etching enhanced PI/PAN@CA/PI three-layer composite separator. The physical blending of CA and PAN reduces the fiber diameter, reduces the thickness of the separator, and increases the contact surface area between the separator and the electrolyte. In addition, the PI/PAN@CA/PI separator was subjected to alkali etching at the same concentration and different times, with more -COOH and -OH groups exposed on the PI and PAN@CA surfaces, greatly improving the electrolyte affinity and ion conductivity of the separator. In the tests after assembly into the battery, the feasibility of alkali etching method enhancing the application of PI/PAN@CA/PI three-layer composite separator in lithium-ion batteries was also verified.

2. Experimental

2.1 Materials

The Polyacrylonitrile (PAN), Cellulose acetate (CA), Sodium hydroxide (NaOH), Pyromellitic dianhydride (PMDA), 4,4'-Diaminodiphenyl ether (ODA), glycerol, dibutyl dicarboxylate, N, N-Dimethylformamide (DMF), Ethanol, Acetic Acid and 1-Butanol were supplied by Shanghai Maclean Biochemical Technology (China), lithium cobaltate cathode ($LiCoO_2$), lithium iron phosphate cathode ($LiFePO_4$), lithium metal anode (Li), 1 mol L^{-1} lithium hexafluoroposphate ($LiPF_6$)/ethylene carbonate (EC) + diethyl carbonate (DEC) + dimethyl carbonate (DMC) mixed electrolyte (EC: DEC: DMC = 1:1:1 vol%) were provided by Guangdong Canrd New Energy Technology Co., Ltd. (China)., which were analytically pure and do not require further purification.

2.2 Preparation of the separators

2.2.1 Preparation of PAN@CA separator

The PAN and AC were weighted with 6.55 g and 2.50 g and separately added in a beaker. And then, the DMF solution with 50 mL was added and stirred in a water bath at 50℃ for 8 h, which was dissolved completely to obtain 12 wt% PAN solution and 5 wt% CA solution. The obtained PAN and CA solution were added with 15:1 volume ratio to a beaker, which was stirred for 5 hours to obtain PAN@CA spinning solution. Afterwards, the PAN@CA separator was fabricated via electrostatic spinning machine (ET-3556H, Beijing Yongkang Leye Technology Development Co., Ltd., China), the spinning parameters were set as follows: the negative voltage was − 1.5 kV; the positive voltage was 15 kV; the speed was 50 rpm; and the distance was only 15 cm with spinning speed 0.2 mm min^{-1}. The operating temperature and humidity were kept at 30℃ and 30%, respectively. The fabricating separator was placed in an oven, which was dried at 60℃ for 3 h to remove residual solvent.

2.2.2 Preparation of PAA non-solvent phase separation separator

The ODA and PMDA were separately added to the three-neck flask with 1:1.01 molar ratio in batches, the appropriate amount of DMF was added to fabricate 15 wt% of PAA solution under ice bath conditions. And then, the 29 wt% pore-making agent was added to the PAA solution, in which the mass ratio of glycerol to dibutyl phthalate was 6:5, which was obtained 10.7 wt% of PAA cast separator solution. The deionized water and anhydrous ethanol with 2:3 volume ratio was utilized in the coagulation bath. The cast separator solution was poured onto the isolation paper, and then immersed into the solidification bath for 15 min, together with the isolation paper to obtain a wet separator.

2.2.3 Preparation of PI/PAN@CA/PI triple-layer composite separator

The PAN@CA separator was sandwiched between two wet PAA separators, which was pressed for 1 min and dried at room temperature for 3 h to obtain PAA/PAN@CA/PAA composite membranes. The dried PAA/PAN@CA/PAA membranes were placed into a tube furnace and heated at 100, 170, and 250℃ for 1 h, respectively, aiming to obtain PI/PAN@CA/PI sandwich separator.

2.2.4 Preparation of alkali etched PI/PAN@CA/PI three-layer composite separator

The PI/PAN@CA/PI separator was soaked in a 7% NaOH aqueous solution for 1, 3, 5, 10, and 30 min, respectively. And then, it was rinsed with large amounts of deionized water to remove extra NaOH. It was soaked in 1% acetic acid solution for 30 min, and finally rinsed again with deionized water until the pH of the rinse solution was 7. The separator was dried in a 50 ℃ oven for 12 h, which was obtained an PI/PAN@CA/PI three-layer composite separator via alkali etching process.

2.3 Material characterizations

The morphology of the composite separator samples was observed to utilize with field emission scanning electron microscope (FE-SEM, Apreo 2S), and the pore size and fiber diameter were measured using Nano Measurer software. Fourier transform infrared spectroscopy (FT-IR, Thermo Fisher iS50R) was analyzed the chemical structure within the range of 400 to 4000 cm^{-}. The element compositions of the samples were qualitatively analyzed using an X-ray photoelectron spectrometer (XPS, ESCALAB Xi). The mechanical strength of the composite separator was investigated using an electronic universal testing instrument (Inspekt Table Blue 5 KN) with a tensile speed of 1 mm min^{-1}. The electrolyte wettability of the separator was evaluated through video optical contact angle meter (Dataphysics OCA100). The thermal stability of the separator was evaluated through thermogravimetric-differential scanning calorimeter (TG-DSC, Netzsch STA449F5).

The percentage porosity of the separator was determined by absorption measurement with n-butanol, which can be calculated by the following Eq. (1):

$$\text{Porosity } \% \ = \frac{W_w - W_d}{\rho V} \times 100\% \ 1$$

Where ρ is the density of n-hexadecane, V is the volume of the separator, W_d is the weight of the dry membrane, and W is the weight of the wet membrane containing n-hexadecane.

The electrolyte absorption (EU) of the separator was determined through the electrolyte adsorption method, which can be calculated by the following Eq. (2):

$$\text{EU } \% \ = \frac{W_1 - W_0}{W_0} \times 100$$

Where W_0 and W_1 are the weight of the dry separator before and after immersing in the electrolyte for 2 h, respectively.

The electrolyte retention rate (ER) was calculated using Eq. (3):

$$\text{ER } \% \ = \frac{W_x - W_0}{W_1 - W_0} \times 100$$

Where W_X is the weight of the separator completely immersed in the electrolyte for 2 h, and then placed in the oven at 25°C. It was weighed at 10 min intervals.

2.4 Cell assembly and electrochemical characterizations

The ionic conductivity of the separator was determined by electrochemical impedance spectroscopy (EIS) using an electrochemical workstation (CHI760E, Shanghai C&H Instruments, China). In accordance with the cell during assembling process, the lithium tablet were replaced with stainless steel spacers (SS) and

assembled into "SS/separator/SS" button cells. The test frequency range was within 10^{-1}-10^{4} Hz accompany with 5 mV amplitude. The ionic conductivity (σ) was calculated using the Eq. (4):

$$\sigma = \frac{d}{Rb \times S} \quad 4$$

Where d is the thickness of the separator sample (cm), R_b is the volume resistance of the separator and electrolyte system (Ω), and S is the area of the separator (cm^2).

The stainless steel spacer (SS) was replaced with lithium tablet (Li) and assembled into a "Li/separator/Li" button cell to investigate the interfacial impedance between the electrolyte separator and the lithium metal by EIS. The testing frequency range is 2×10^{-2}-10^{6} Hz.

To evaluate the electrochemical stability of separator absorbing liquid electrolyte, the cell with Li/separator/SS structure was measured by linear scanning voltammetry (LSV) with 1 mol L^{-1} $LiPF_6$ in 1:1 EC/DEC, the lithium metal as the negative electrode, and SS as the positive electrode. The scanning speed was 5 mV s^{-1}, and the scanning potential was 4.0–6.0 V.

To evaluate the electrichemical performance of lithium-ion batteries equipped with different separators, the cycling performance of the batteries were measured by cycling 100 times at 1 C discharge rate. The rating performance of the batteries was evaluated at different discharge rates such as 0.1 C, 0.5 C, 1 C, 2 C, and 5 C, respectively.

3. Results and discussion

3.1 Physical properties characterization

Owing to the requirement for 250°C heat treatment during the preparation of PI/PAN@CA/PI separator, aimed to investigate the effects of adding CA on the morphology and structure of PAN, TF-SEM was utilized to record the PAN and PAN@CA after gradually heating treatment. The PAN and PAN@CA after heating treatment were denoted as PAN-T and PAN@CA-T, respectively. As shown in fig (a) and (c), from the microstructure, the fibers became finer and the pores between the fibers became larger after the addition of CA. The fiber diameter analysis of the samples was performed through Nano Measure software. As described in Fig. 2 (b) and (d), the average fiber diameter is decreased from 357.95 nm to 265.11 nm when CA was added. The main reason is that CA can reduce the viscosity of PAN spinning solution owing to the intermolecular entanglement[24]. The specific surface area is increased when the fiber diameter increased to a certain degree, which can increase the contact area between the separator and the electrolyte. It is benefited to improve the stability of the lithium ions transportation process.

In order to investigate the degree of alkali etching of PI at different times during alkali etching process, TF-SEM has been utilized to characterize the outer layers of PI after alkali etching for 0, 1, 3, 5, 10, and 30 min. As shown in Fig. 3 (a) and (b), when the alkali etching time of PI/PAN@CA/PI separator after 3 min,

the separator is maintained original pore structure, with less significant changes. When the alkali etching time increased to 5 min, there is obvious dissolution on the surface of the separator, and the pores size is increased. After the dissolution of the internal pores, which are not easily carried away by the alkali solution and remain inside the separator, making it easy to plug the pore gaps. As depicted in Fig S1 (a) and (b), the pores on the surface and cross-section of PI show obvious dissolution and blockage after alkaline etching 10 min and 30 min, and the integrity pore structure is severely destroyed. The pore structure of separator can affect the electrolyte absorbing rate, electrolyte retention rate, and cycling performance of battery with the separator. Therefore, the alkali etching time should be controlled within 5 min to ensure the mechanism performances of the separator.

In Fig. 4 (a), it reveals the infrared spectrum exhibits characteristic peaks of PI such as C = O asymmetric stretching vibration at 1780 cm^{-1}, C = O symmetric stretching vibration at 1725 cm^{-1}, C-N-C stretching vibration at 1370 cm^{-1}, and C = O deformation vibration at 725 cm^{-1} before and after alkali etching[25], which indicates that the characteristics of PI are maintained after alkali etching. However, compared with the characteristic peaks of the imide ring at 1780 cm^{-1} and 1370 cm^{-1}, it reveals that the imide ring characteristic peaks are gradually weaken, while the amide bond's characteristic peaks (C = O and N-H bond) at 1653 cm^{-1} and 1542 cm^{-1} are increased with the increase of alkali etching time. Besides, the tensile vibration peak of -OH in the -COOH group at 3000–3700 cm^{-1} increases accompany with the increase of alkali etching time. It indicates that the imide ring on the surface can be opened without destroying the primary characteristics of PI in 7 wt% NaOH aqueous solution for 5 min after alkali etch, which can produce much -COOH to benefit the contact with electrolyte[26]. In Fig. 4 (b), it shows that the oxygen content of the PI separator without alkali etching technology is 17.63% in the XPS diffraction spectrum. The oxygen content with alkali treatment times of 0, 1, 3, and 5 min are 17.63%, 20.67%, 21.29%, and 23.11%, respectively. The surface oxygen content of PI is determined by the amount of -COOH, which is increased alkaline etching time that can promote the exposure of much -COOH on the PI surface at a certain range[27]. Figure 4 (c) shows the chemical reaction formula of PI alkali etching process, which is mainly involved to open the imide ring of PI to expose -COOH on the surface of the PI separator. If the alkali etching degree is too high, the PI will be decomposed into diamine and dianhydride monomers[28, 29]. Thus, the alkali etched with 5 min is suitable to produce much porous structure to improve the electrochemical performance of separator. To visually demonstrate the changes of hydrolysis on the separator, Fig. 4 (d) briefly showed the changes in the outer and inner layers of the PI/PAN@CA/PI separator after alkali etching.

Besides, the component analysis were performed on the PAN@CA fiber portion, as shown in the infrared spectrum of Fig. 5 (a). The characteristic peaks of CA appeared at 1681, 1330, and 1245 cm^{-1}, which are corresponded to the stretching vibration of carbonyl (C = O), CH, and ester bond (OC = O), respectively[30]. Moreover, the characteristic peaks of PAN are corresponded to 2936, 2243, 1453, and 1067 cm^{-1}, respectively, which are presented to the tensile vibration of C-H_2, the tensile vibration of C ≡ N, the bending vibration of C-H_2 and the deforming peak of C-H[31]. The characteristic peaks corresponding to

CA and PAN can be completely found on PAN@CA, and no new absorption peaks have been formed. This indicates that the blending of PAN and CA is uniform and belongs to physical blending. As shown in the energy spectrum of Fig. 5 (b), the N element of PAN and the O element of CA are uniformly dispersed on the fiber, further demonstrating the uniform blending of PAN and CA.

As shown in Fig. 5 (a), the infrared spectrum shows that PAN@CA exhibits new absorption peaks at 1613 cm^{-1} and 1280 cm^{-1} after heat treatment, corresponding to the tensile vibrations of C = C and C-N. At the same time, the intensity of the bending vibration absorption peak of C-H_2 at 2243 cm^{-1} and 1453 cm^{-1} decreased significantly, which is attributed to the cyclization, dehydrogenation, and oxidation reactions during the thermal stabilization process[32]. This can be explained from the reaction equation of PAN thermal stabilization process in Fig. 5 (c). In addition, PAN and the products of the thermal stabilization process underwent cyclization after mild alkali etching, exposing hydroxyl groups, and the cyclized portion continues to hydrolyze to produce carbonyl groups[33]. The ester group of CA was easily hydrolyzed into hydroxyl groups during alkaline etching[20].

In order to verify the effect of alkali etching on PAN@CA, the infrared spectra of PAN@CA under different alkali etching times were further measured. The infrared spectrum is shown in Fig. 6 (a), and with the extension of alkali etching time, a wide peak appears at 3500 cm^{-1}. The appearance of this absorption peak is attributed to the hydrolysis of CA ester groups into -OH groups, as well as the hydrolysis of PAN and its thermal stabilization products[23]. The strengthening of the C = C vibration absorption peak at 1613 cm^{-1} also corresponds to the strengthening of the cyclization reaction.

To further validate the introduction of hydroxyl groups (-OH) into the surface of PAN@CA-T by alkali etching, we tested the water contact angle of the separator to investigate the changes in its hydrophilicity, as shown in Fig. 6 (b). It can be seen that the contact angle before alkali etching is 124°, which indicates strong hydrophobicity. However, after alkali etching, the contact angle gradually decreases to 0°, indicating the presence of hydrophilic groups on the surface of the separator[20]. This is attributed to the hydrolysis reaction.

To observe the performance changes of PI/PAN@CA/PI after alkali etching, thermogravimetric analysis was conducted. As shown in Fig. 7 (a), it can be seen that the PP separator begins thermal decomposition at 400℃ until complete decomposition is achieved, and only 1.84% of the remaining mass remains, which is in line with the thermal decomposition law of polypropylene. From the thermal weight loss curve of the PI/PAN@CA/PI separator after alkali etching for 0 min, the first turning point is around 250℃. This is because the CA in the separator begins to decompose after reaching the melting temperature around 300℃, and the PAN component also begins to participate in the thermal decomposition stage. The second inflection point is around 550℃, which is because the PI molecular skeleton decomposition temperature has been reached, and the final thermal weight loss reaches 51.36%, indicating that the separator has good thermal performance.

Compared with the TG curves of separators etched with alkali for 0, 1, 3, and 5 min, it is obvious that alkali etching reduces the thermal performance of the separator, which is particularly evident at 250℃ in the first stage, where the thermal weight loss ratio increases. This is because the imide ring opens during the alkali etching process of PI, forming a structure similar to polyamide acid[34]. Therefore, dehydration occurs around 250℃, leading to an increase in thermal weight loss. The DTG curve in Fig. 7 (b) shows that PAN@CA-T exhibits a significant peak at 280–410℃, which is consistent with the thermal decomposition temperature of CA and the thermal stabilization reaction of PAN. At the same time, the thermal performance of PAN@CA-T also decreases after alkali etching, leading to an increase in the overall separator's thermal weight loss. However, even after 5 min of alkali etching, there is still 48.4% remaining mass in the separator after heating, indicating that the separator still has good thermal performance.

As shown in Fig. 7 (c), it can be seen that the PP separator almost disappears after combustion, indicating a lack of flame retardancy. Comparing the pre- and post-combustion states of PI/PAN@CA/PI separators after different alkali etching times, it can be found that the separator immediately stops burning after the open flame is extinguished and retains most of the diaphragm without being completely burned out. As the alkali etching time increases, the remaining part after combustion decreases, indicating a decrease in flame retardancy. This is because the flame retardancy of the outer layer of PI is provided by the imide ring on the main chain, and the ring opening reaction occurs during alkali etching, reducing the flame retardancy of PI[28, 34]. However, as the alkali etching time is relatively short, it does not have a significant impact on the overall thermal performance of PI/PAN@CA/PI, and the separator still maintains high thermal stability.

As shown in the stress-strain curve in Fig. 7 (d), the tensile strength of the PI/PAN@CA/PI three-layer composite separator decreases as the alkali etching time increases. After 0, 1, 3, and 5 min of alkali etching, the tensile strength is 20.1, 18.6, 17.8, and 15.4 MPa, respectively. This is because the tensile strength of PI/PAN@CA/PI is mainly determined by the PI in the outer layer. When PI is etched in alkali, the imide ring opens, reducing the molecular weight of PI to some extent, resulting in a reduction in tensile strength[35].

Table 1 shows that the porosity of the composite separator slightly increases after alkali etching, followed by a decrease. This may be because during the alkali etching process, some PI is hydrolyzed and removed, resulting in larger pores and an increase in porosity. As the alkali etching time prolongs, the hydrolyzed PI cannot be removed in time, leading to pore blockage and a decrease in porosity. However, because of the short hydrolysis time, the overall change is not significant.

Table 1
Physical and chemical properties of PP separator and PI/PAN@CA/PI separator with alkali etching at different times

Sample	Thickness (μm)	Ionic conductivities(mS cm^{-1})	porosity(%)	Electrolyte uptake (%)	Electrolyte retention (%)
PP	25	0.18	47.3	194.4	27.7
0 min	50	0.50	81.7	358.2	76.3
1 min	50	0.57	82.1	448.8	78.6
3 min	50	1.22	82.4	474.9	82.4
5 min	50	0.73	80.2	463.6	80.2

As shown in Fig. 8 (a), after dropping the electrolyte for 5 min, it can be observed that the electrolyte on the surface of PP has a little wetting with contact angle of 48°, indicating poor electrolyte wettability. Observing the PI/PAN@CA/PI separators with alkali etching for 0, 1, 3, and 5 min, it can be seen that as the alkali etching time increases, more electrolytes diffuse, and the contact angle decreases to 0°. This is because alkali etching exposes the -COOH on the surface of the PI membrane of the PI/PAN@CA/PI separator, improving the electrolyte's wettability [27].

As shown in Fig. 8 (b) and (c), the electrolyte absorption and retention rates of the PP separator and the PI/PAN@CA/PI separator after alkali etching for 0, 1, 3, and 5 min are 194.4, 358.2, 448.8, 474.9, and 463.6%, as well as 27.7, 76.3, 78.6, 82.4, and 80.2%, respectively. It can be seen that the PI/PAN@CA/PI separator after 3 min of alkali etching has the best electrolyte absorption and retention rate. This is because, under the effect of alkali etching, the PI layer is forced to open the imide ring, exposing more -COOH and providing more interaction sites with the electrolyte, which improves the electrolyte affinity. Appropriate alkali etching can ensure that the unique pore structure of the PI/PAN@CA/PI separator will not be damaged.

The PI/PAN@CA/PI three-layer composite separators were assembled after alkali etching for 0, 1, 3, and 5 min into a "SS/separator/SS" button cell for electrochemical impedance testing, respectively. As shown in Fig. 9 (a), the electrochemical impedance of the PI/PAN@CA/PI separator assembly battery after alkali etching for 0, 1, 3, and 5 min was 3.9, 3.4, 1.6, and 2.7 Ω, respectively. As the alkali etching time continued to increase, the electrochemical impedance first decreased and then increased. The PI/PAN@CA/PI separator has the lowest electrochemical impedance at 3 min of alkali etching, which is much lower than the 5.2 Ω of commercial PP separators.

According to formula (3), the PI/PAN@CA/PI separator with 3 min of alkaline etching has the highest ion conductivity, reaching 1.22 mS cm^{-1}, which is much higher than the 0.18 mS cm^{-1} of commercial PP film. A "Li/separator/Li" button battery was assembled for testing. Figure 9 (b) shows the interface impedance diagram of the PI/PAN@CA/PI separator after PP and alkali etching for 0, 1, 3, and 5 min. It

can be observed that the interface impedance between the PI/PAN@CA/PI separator and the electrode after alkali etching for 0, 1, 3, and 5 min is 248, 200, 152, and 172 Ω, respectively. As the alkali etching time prolongs, the interface resistance first decreases and then increases, which is consistent with the change in electrochemical impedance. The PI/PAN@CA/PI separator after 3 min of alkali etching has the lowest interface resistance, which is much lower than the 400 Ω of commercial PP separators.

The lower interface resistance indicates that the separator has better interface compatibility with the electrolyte and electrode. In battery operation, Li^+ can quickly shuttle between the electrode, electrolyte, and separator interfaces, thereby improving the capacity performance of the battery. The mechanism analysis is shown in Fig. 9 (c). The excellent ion conductivity and low interface impedance are attributable to the unique structure of the PI/PAN@CA/PI composite separator and the effect of alkali etching, which improves the wettability and surface characteristics of the separator and enhances its ability to transport lithium ions[26].

To test the influence of alkali etching time on the electrochemical stability of the separator, a "Li/separator/SS" button cell was assembled. The linear voltammetric scanning curves of the PI/PAN@CA/PI separator were measured after alkali etching for 0, 1, 3, and 5 min to study the changes in the electrochemical stability window. As shown in Fig S2, it can be observed that the electrochemical stability window of the PI/PAN@CA/PI separator decreases slightly with increasing alkaline etching time but remains at high electrochemical stability (> 5.2 V), which is greater than the 5.0 V of commercial PP separators.

The change in the electrochemical stability window is attributable to the effect of alkali etching on the PI/PAN@CA/PI separator, which not only improves the electrochemical performance but also affects the chemical stability of the separator. However, the alkaline etching time is relatively short, and the electrochemical stability remains at a high level, which can adapt to the redox reaction of the battery in the charge and discharge process and has good safety performance.

As shown in Fig. 10(a), The "$LiCoO_2$/separator/Li" battery using PP separator and PI/PAN@CA/PI separator after 0, 1, 3, and 5 min of alkali etching were charged and discharged 100 times at a current density of 1 C, resulting in remaining capacities of 115, 129, 131, 141, and 135 mAh g^{-1}, respectively. The capacity retention rates were 82.1%, 92.1%, 93.4%, 95.3%, and 93.8%, respectively. As shown in Fig. 10(c) and (d), the discharge specific capacities of batteries using PI/PAN@CA/PI separator after 0, 1, 3, and 5 min of alkali etching at 0.1 C and 5 C are 163.1, 163.3, 166.9, and 163.1 mAh g^{-1}, as well as 86.3, 87.1, 114.9, and 96.8 mAh g^{-1}, respectively. It can be seen that the capacity change of the battery is relatively small at low magnification, while the capacity change at high magnification significantly increases and then decreases with the alkali etching time. The battery has the highest discharge specific capacity at 3 min of alkali etching. As shown in Fig. 10(b), at current densities of 0.1, 0.2, 0.5, 1, 2, and 5 C, the discharge specific capacities of the battery assembled by the PI/PAN@CA/PI separator after alkali etching for 3 min are 166.9, 166.1, 160.8, 152.8, 140.1, and 114.9 mAh g^{-1}, respectively, which are superior to the initial PI/PAN@CA/PI separator's 163.1, 159.3, 153.9, 145.2, 125.7, and 86.3 mAh g^{-1}, and

much higher than the commercial PP separator's 160.5, 154.8, 148.8, 149.6, 118.8, and 77.1 mAh g^{-1}. As shown in Fig S3, the half-cell assembled by the PI/PAN@CA/PI separator after 3 min of alkaline etching has a similar charge and discharge capacity at various magnification rates and has high coulombic efficiency. Overall, the PI/PAN@CA/PI separator after 3 min of alkaline etching has the highest discharge specific capacity and capacity retention rate, indicating excellent cycling performance and rate discharge performance. Thanks to the unique dual pore structure of the separator, it is beneficial to preserve more electrolyte and prevent leakage. Meanwhile, the improved affinity of -COOH and -OH to the separator electrolyte caused by alkaline etching allows for rapid and stable transmission of lithium ions between electrodes, thereby improving battery safety and stability[20, 27]. However, a certain period of alkaline etching can cause the outer layer of PI to dissolve to some extent, blocking the pores, increasing internal resistance, hindering the movement of lithium ions between the electrodes, and reducing battery performance. Therefore, controlling the time of alkaline etching is necessary to achieve the optimal state of the separator.

4. Conclusions

The growing demand for thermal safety and energy in lithium-ion batteries is a major challenge. In this study, an alkali etching enhanced PI/PAN@CA/PI three-layer composite separator was designed. It was found that the addition of CA reduced the fiber diameter of PAN and the overall thickness of the PI/PAN@CA/PI composite separator. At the same time, CA underwent a certain amount of melting after heat treatment which increased fiber viscosity and enhanced a certain degree of mechanical strength. With the continuous increase of alkali etching time, the PI ring opening reaction gradually intensified and the surface -COOH groups increased. At the same time, pores dissolved and were then blocked, and mechanical strength and thermal performance decreased as well. When the alkali etching time was 3 min, PI/PAN@CA/PI had the best electrochemical performance, with an ion conductivity of 1.22 mS cm^{-1} and an interface impedance of 152 Ω. After 100 cycles of charging and discharging at a current density of 1 C, the capacity retention rate was 95.3%. At a current density of 5 C, the specific capacity of charging and discharging reached 114 mAh g^{-1}, which was better than the 87.3 mAh g^{-1} of the initial PI/PAN@CA/PI separator. These excellent properties indicate that a certain degree of alkaline etching can increase the -COOH and -OH groups on the surface of PI and PAN@CA, greatly increasing the electrolyte affinity of the separator, enhancing the migration rate of lithium ions between electrodes, and thus improving battery performance. In addition, this alkali etching modification method has a simple operation process, low cost, and great industrial production potential.

Declarations

CRediT authorship contribution statement

Declaration of competing interest

The authors declare that they have no known competing financial interests or personal relationships that could have appeared to influence the work reported in this paper.

Acknowledgments

This research was financially supported by Basic and applied basic research projects of Guangzhou city (202201010050 and 202201010226).

References

1. Yang Y, Wang W, Meng G, et al. Function-directed design of battery separators based on microporous polyolefin membranes[J]. Journal of Materials Chemistry A. 2022, 10(27): 14137–14170.
2. Liu Y, Li C, Li C, et al. Highly Thermally Stable, Highly Electrolyte-Wettable Hydroxyapatite/Cellulose Nanofiber Hybrid Separators for Lithium-Ion Batteries[J]. ACS Applied Energy Materials. 2023, 6(7): 3862–3871.
3. Choi J, Kim P J. A roadmap of battery separator development: Past and future[J]. Current Opinion in Electrochemistry. 2022, 31: 100858.
4. Dai X, Zhang X, Wen J, et al. Research progress on high-temperature resistant polymer separators for lithium-ion batteries[J]. Energy Storage Materials. 2022, 51: 638–659.
5. Yu J, Dong N, Liu B, et al. A newly-developed heat-resistance polyimide microsphere coating to enhance the thermal stability of commercial polyolefin separators for advanced lithium-ion battery[J]. Chemical Engineering Journal. 2022, 442: 136314.
6. Xie Y, Chen X, Han K, et al. Natural halloysite nanotubes-coated polypropylene membrane as dual-function separator for highly safe Li-ion batteries with improved cycling and thermal stability[J]. Electrochimica Acta. 2021, 379: 138182.
7. Senthilkumar S, Ramasubramanian B, Rao R, et al. Advances in Electrospun Materials and Methods for Li-Ion Batteries[J]. Polymers. 2023, 15: 1622.
8. Ding J, Zhang J, Li J, et al. Electrospun polymer biomaterials[J]. Progress in Polymer Science. 2019, 90: 1–34.
9. Wang Y, Guo M H, Fu H, et al. Thermotolerant separator of cross-linked polyimide fibers with narrowed pore size for lithium-ion batteries[J]. JOURNAL OF MEMBRANE SCIENCE. 2022, 662.
10. Bicy K, Gueye A B, Rouxel D, et al. Lithium-ion battery separators based on electrospun PVDF: A review[J]. Surfaces and Interfaces. 2022, 31: 101977.
11. Gao X X, Sheng L, Yang L, et al. High-stability core-shell structured PAN/PVDF nanofiber separator with excellent lithium-ion transport property for lithium-based battery[J]. JOURNAL OF COLLOID AND INTERFACE SCIENCE. 2023, 636: 317–327.
12. Guo M, Zhu H, Wan P, et al. Freestanding and Ultra-flexible PAN/ZIF-67 Hybrid Membrane with Controlled Porosity for High-Performance and High-Safety Lithium Batteries Separator[J]. Advanced Fiber Materials. 2022, 4(6): 1511–1524.

13. Jung J, Lee C, Yu S, et al. Electrospun nanofibers as a platform for advanced secondary batteries: a comprehensive review[J]. Journal of Materials Chemistry A. 2016, 4(3): 703–750.
14. Lu Z, Sui F, Miao Y, et al. Polyimide separators for rechargeable batteries[J]. Journal of Energy Chemistry. 2020.
15. Zhang H, Lin C, Zhou M, et al. High thermal resistance polyimide separators prepared via soluble precusor and non-solvent induced phase separation process for lithium ion batteries[J]. Electrochimica Acta. 2016, 187: 125–133.
16. Li S, Chen H, Wen M, et al. Preparation of hydrothermally stable, basic, and highly active nano nickel catalysts for the hydrodeoxygenation of N,N-dimethylformamide[J]. Journal of Catalysis. 2016, 338: 1–11.
17. Ma T, Cui Z, Wu Y, et al. Preparation of PVDF based blend microporous membranes for lithium ion batteries by thermally induced phase separation: I. Effect of PMMA on the membrane formation process and the properties[J]. Journal of Membrane Science. 2013, 444: 213–222.
18. Li M, Zhang Z, Yin Y, et al. Novel Polyimide Separator Prepared with Two Porogens for Safe Lithium-Ion Batteries[J]. ACS Applied Materials & Interfaces. 2020, 12(3): 3610–3616.
19. Weng B, Xu F, Alcoutlabi M, et al. Fibrous cellulose membrane mass produced via forcespinning® for lithium-ion battery separators[J]. Cellulose. 2015, 22(2): 1311–1320.
20. Xie X, Sheng L, Arbizzani C, et al. Multi-functional groups decorated composite nanofiber separator with excellent chemical stability in ester-based electrolyte for enhancing the lithium-ion transport[J]. Journal of Power Sources. 2023, 555: 232431.
21. Deng J H, Zhang G Q, Yang X Q, et al. H-Bond Cross-Linked Polyimide Nanofiber-Modified Polyethylene Composite Separators for Lithium-Ion Batteries[J]. SCIENTIA HORTICULTURAE. 2023, 316: 6770–6777.
22. Jin S Y, Kim M H, Jeong Y G, et al. Effect of alkaline hydrolysis on cyclization reaction of PAN nanofibers[J]. Materials & Design. 2017, 124: 69–77.
23. Yang X, Liew S R, Bai R. Simultaneous alkaline hydrolysis and non-solvent induced phase separation method for polyacrylonitrile (PAN) membrane with highly hydrophilic and enhanced anti-fouling performance[J]. Journal of Membrane Science. 2021, 635: 119499.
24. Mahalingam S, Wu X, Edirisinghe M. Evolution of self-generating porous microstructures in polyacrylonitrile-cellulose acetate blend fibres[J]. Materials & Design. 2017, 134: 259–271.
25. Yang T, Han E, Wang X, et al. Surface decoration of polyimide fiber with carbon nanotubes and its application for mechanical enhancement of phosphoric acid-based geopolymers[J]. Applied Surface Science. 2017, 416: 200–212.
26. Deng J, Cao D, Yang X, et al. Cross-linked cellulose/carboxylated polyimide nanofiber separator for lithium-ion battery application[J]. Chemical Engineering Journal. 2022, 433: 133934.
27. Lin C, Zhang H, Song Y, et al. Carboxylated polyimide separator with excellent lithium ion transport properties for a high-power density lithium-ion battery[J]. Journal of Materials Chemistry A. 2018, 6(3): 991–998.

28. Tian G, Chen B, Qi S, et al. Enhanced surface free energy of polyimide fibers by alkali treatment and its interfacial adhesion behavior to epoxy resins[J]. Composite Interfaces. 2016, 23(2): 145–155.
29. Dong G, Liu B, Sun G, et al. TiO2 nanoshell@polyimide nanofiber membrane prepared via a surface-alkaline-etching and in-situ complexation-hydrolysis strategy for advanced and safe LIB separator[J]. Journal of Membrane Science. 2019, 577: 249–257.
30. Chen W, Su Y, Zheng L, et al. The improved oil/water separation performance of cellulose acetate-graft-polyacrylonitrile membranes[J]. Journal of Membrane Science. 2009, 337(1): 98–105.
31. Guo M, Dong S, Xiong J, et al. Flexible core-shell PAN/CNTs@PVDF-HFP/Uio-66-NH2 hybrid nanofibers membrane for advanced lithium-ion batteries separator[J]. Materials Today Chemistry. 2023, 30: 101552.
32. Lee K I, Li J, Fei B, et al. Mechanism study of heat stabilization of polyacrylonitrile nanofibers against alkaline hydrolysis[J]. Polymer Degradation and Stability. 2014, 105: 80–85.
33. Han C, Liu Q, Xia Q, et al. Facilely cyclization-modified PAN nanofiber substrate of thin film composite membrane for ultrafast polar solvent separation[J]. Journal of Membrane Science. 2022, 641: 119911.
34. Wu Z P, Wu D Z, Li F, et al. Surface modification-based fabrication of double surface highly reflective and conductive metallized polymeric films and microstructural tuning nanocomposite layers[Z]. Asian International Conference on Advanced Materials: 2006: 11–12, 497.
35. Gu J, Zhang K, Li X, et al. Construction of Safety and Non-flammable Polyimide Separator Containing Carboxyl Groups for Advanced Fast Charing Lithium-ion Batteries[J]. Chinese Journal of Polymer Science. 2022, 40(4): 345–354.

Figures

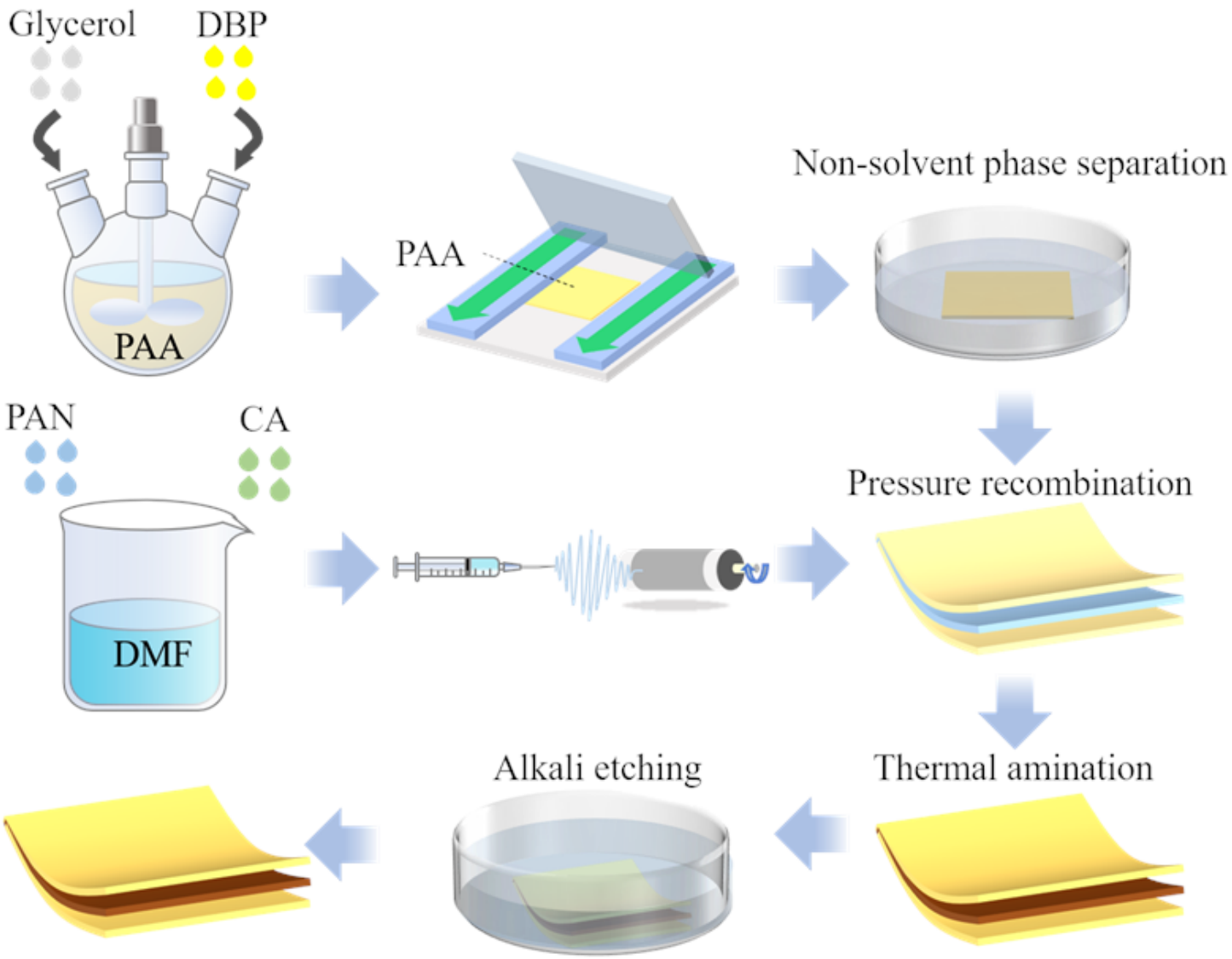

Figure 1

The preparation process of PI/PAN/PI separator

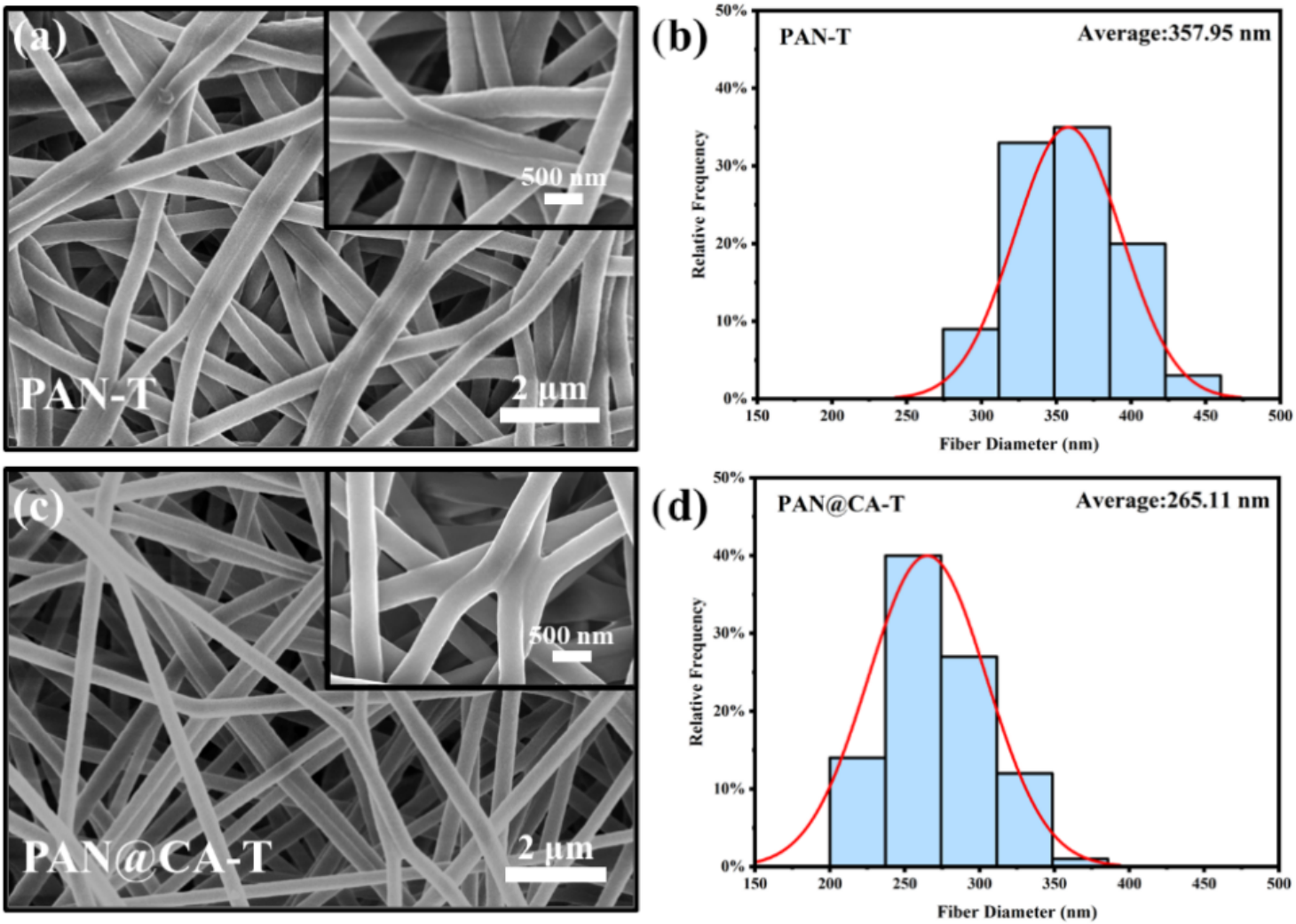

Figure 2

(a) and (c) SEM images of PAN and PAN@CA after heat treatment at 250 °C respectively; (b) and (d) Fiber diameter images of PAN and PAN@CA after heat treatment at 250 °C respectively.

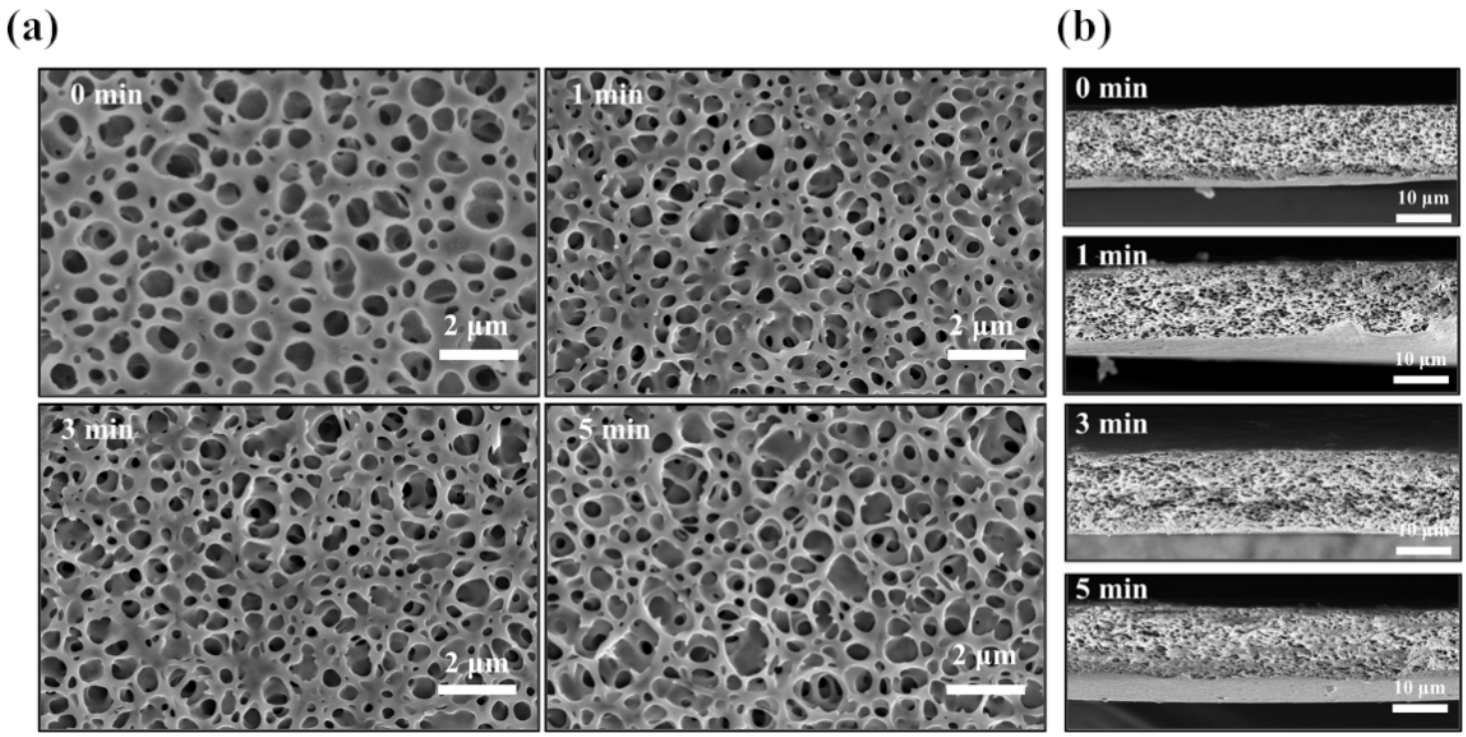

Figure 3

(a) SEM surface image of the PI outer separator after alkali etching for 0, 1, 3, and 5 min; (b) SEM cross-sectional images of the PI outer separator after alkali etching for 0, 1, 3, and 5 min.

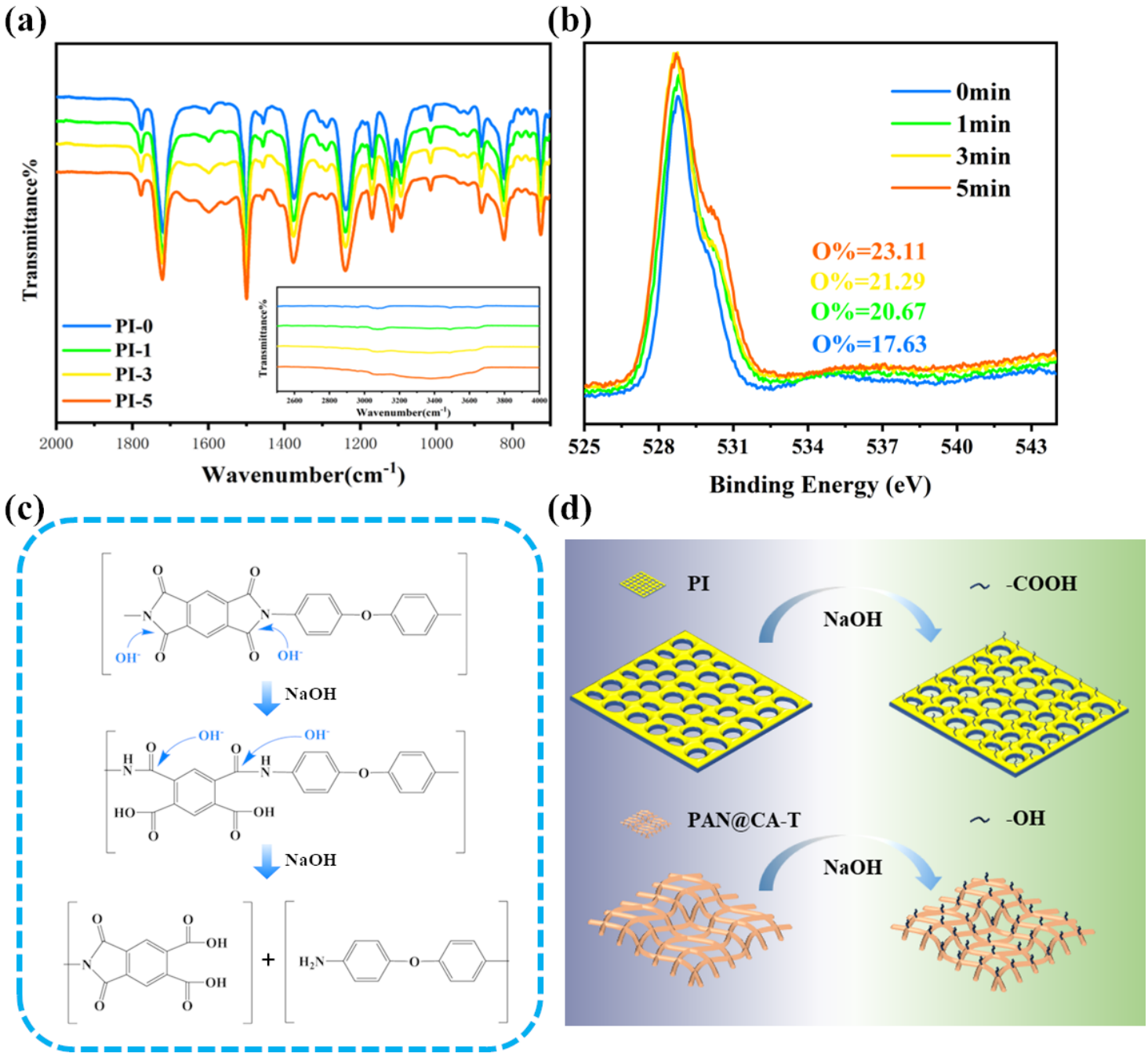

Figure 4

(a) Fourier transform infrared spectroscopy; (b) XPS diffraction O content spectrum; (c) Possible reaction chemical formula for PI alkali etching after 0, 1, 3, and 5 min of PI alkali etching; (d) Schematic diagram of the hydrolysis changes in the outer and inner layers.

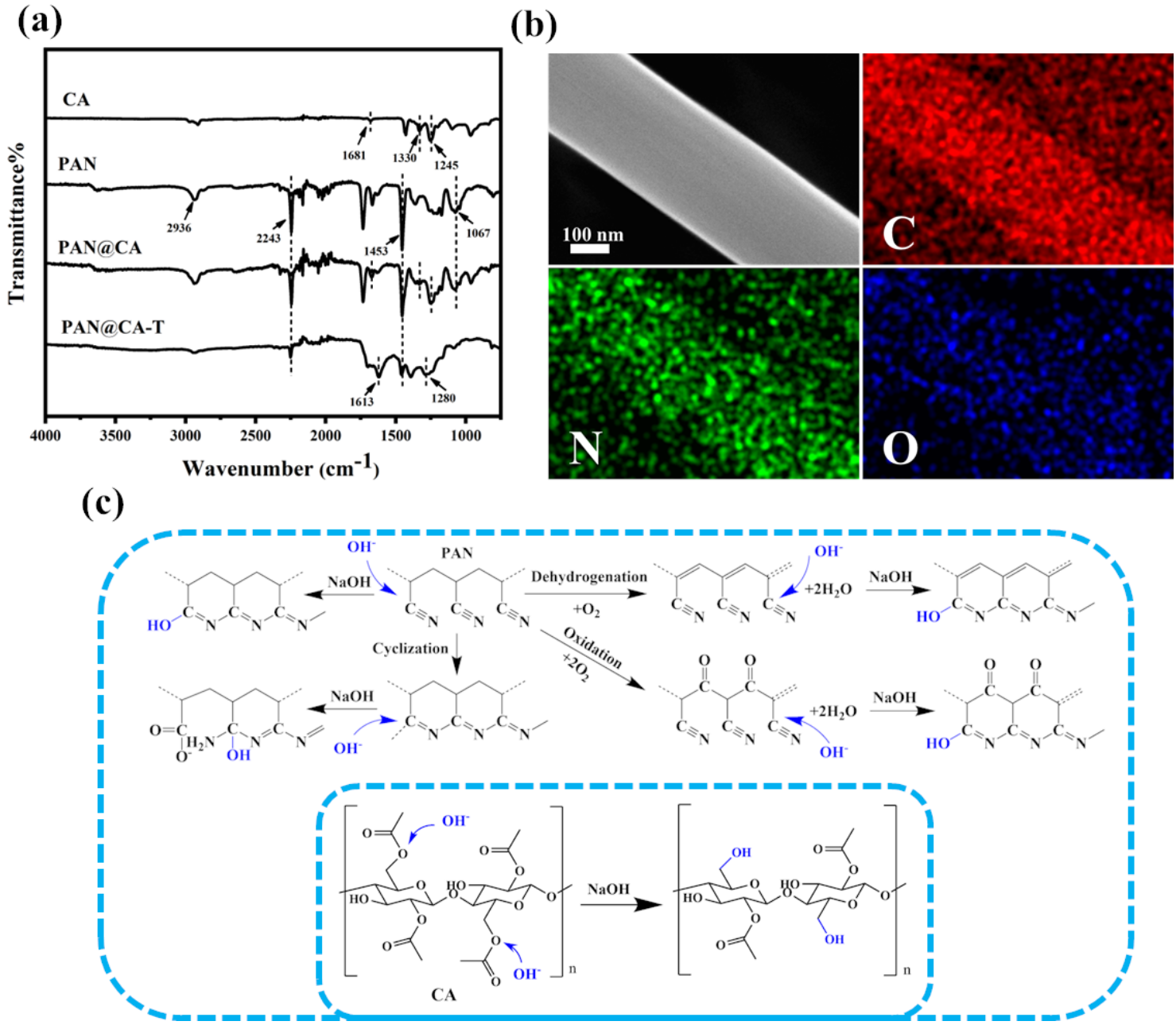

Figure 5

(a) Infrared spectra of CA, PAN, PAN@CA, and PAN@CA-T; (b) EDS energy spectrum element distribution of PAN@CA; (c) Chemical formulas for reactions that may occur after thermal stabilization of PAN and CA alkali etching

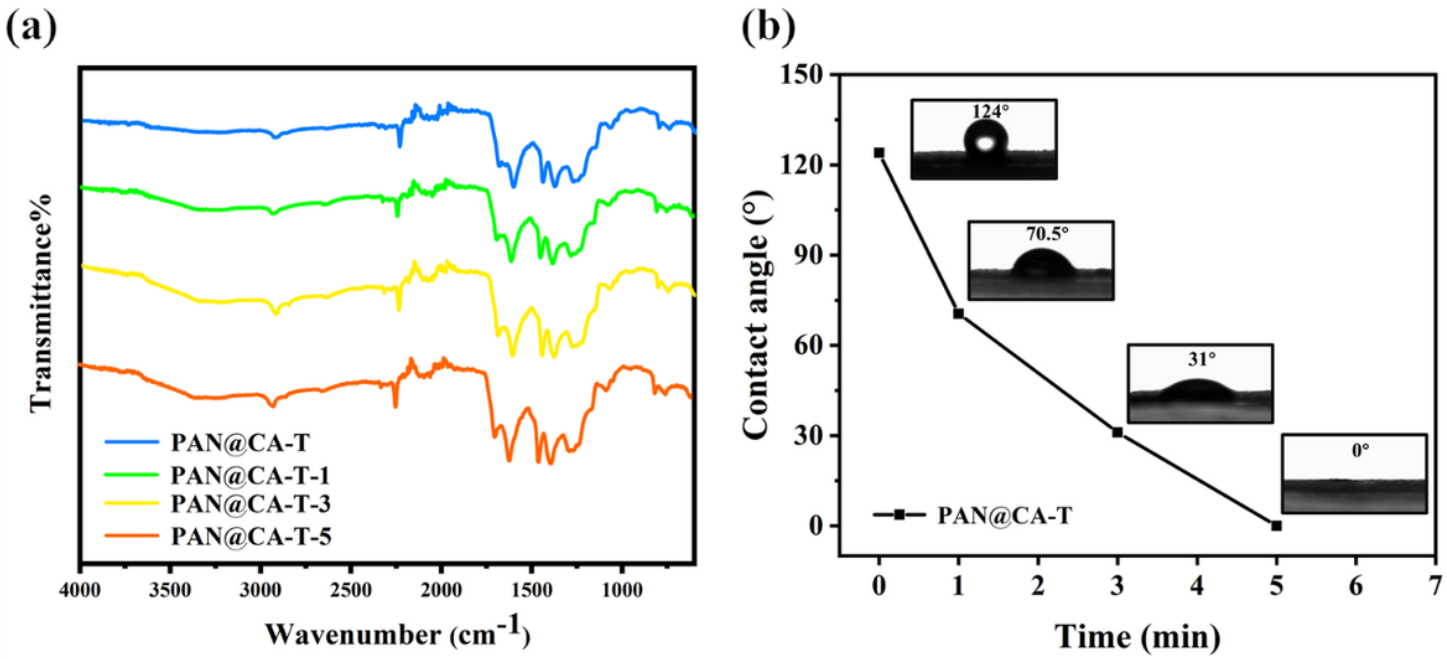

Figure 6

(a) Infrared spectra of PAN@CA-T after alkaline etching for 0, 1, 3, and 5 min; (b) Water contact angle of PAN@CA-T after alkaline etching for 0, 1, 3, and 5 min.

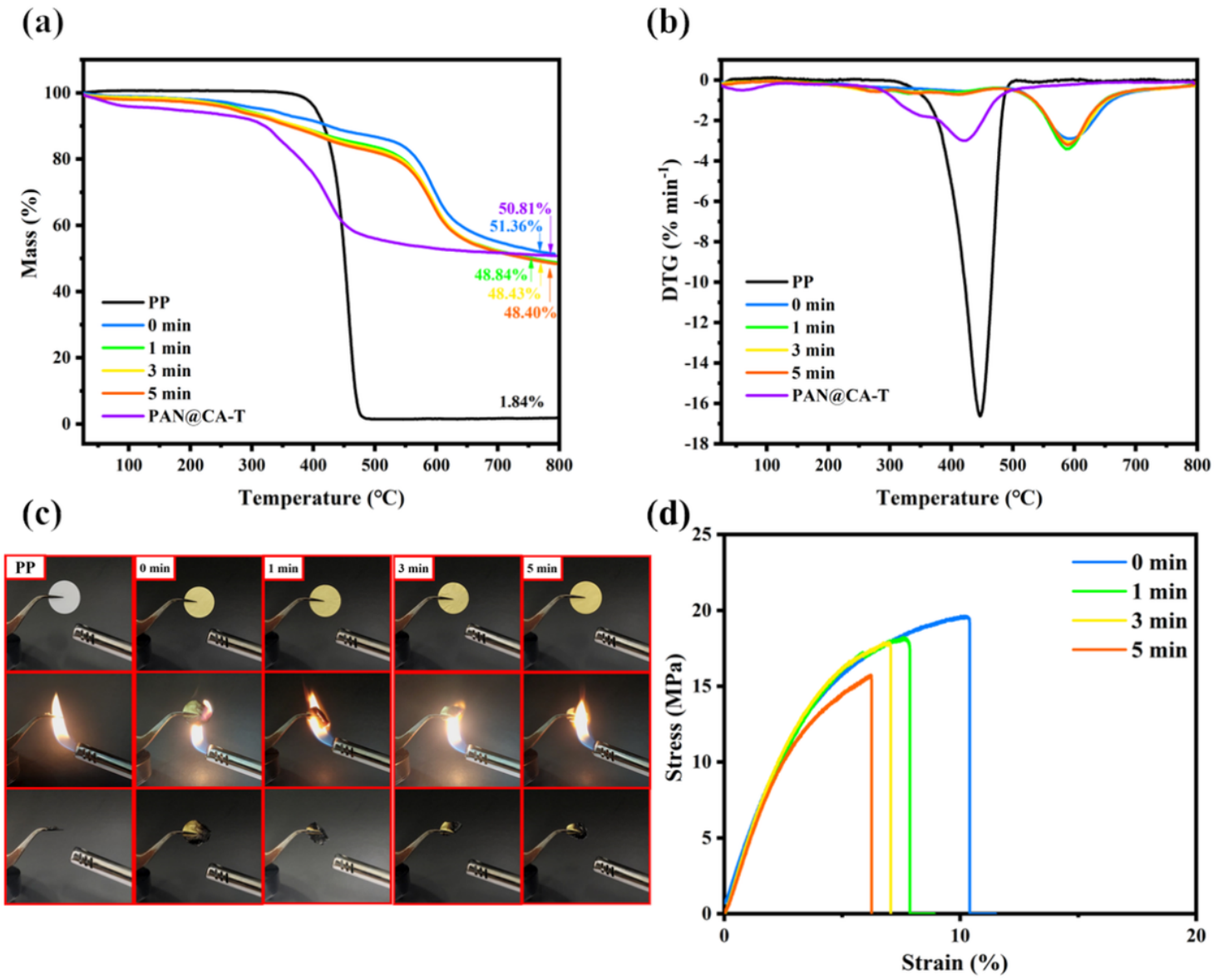

Figure 7

(a) TG curves and (b) DTG curves of PI/PAN@CA/PI and PAN@CA-T after 0, 1, 3, and 5 min of PP separator and alkali etching; PP separator and PI/PAN@CA/PI after 0, 1, 3, and 5 min of alkali etching (c) flame retardant experiment (d) tensile strength curve.

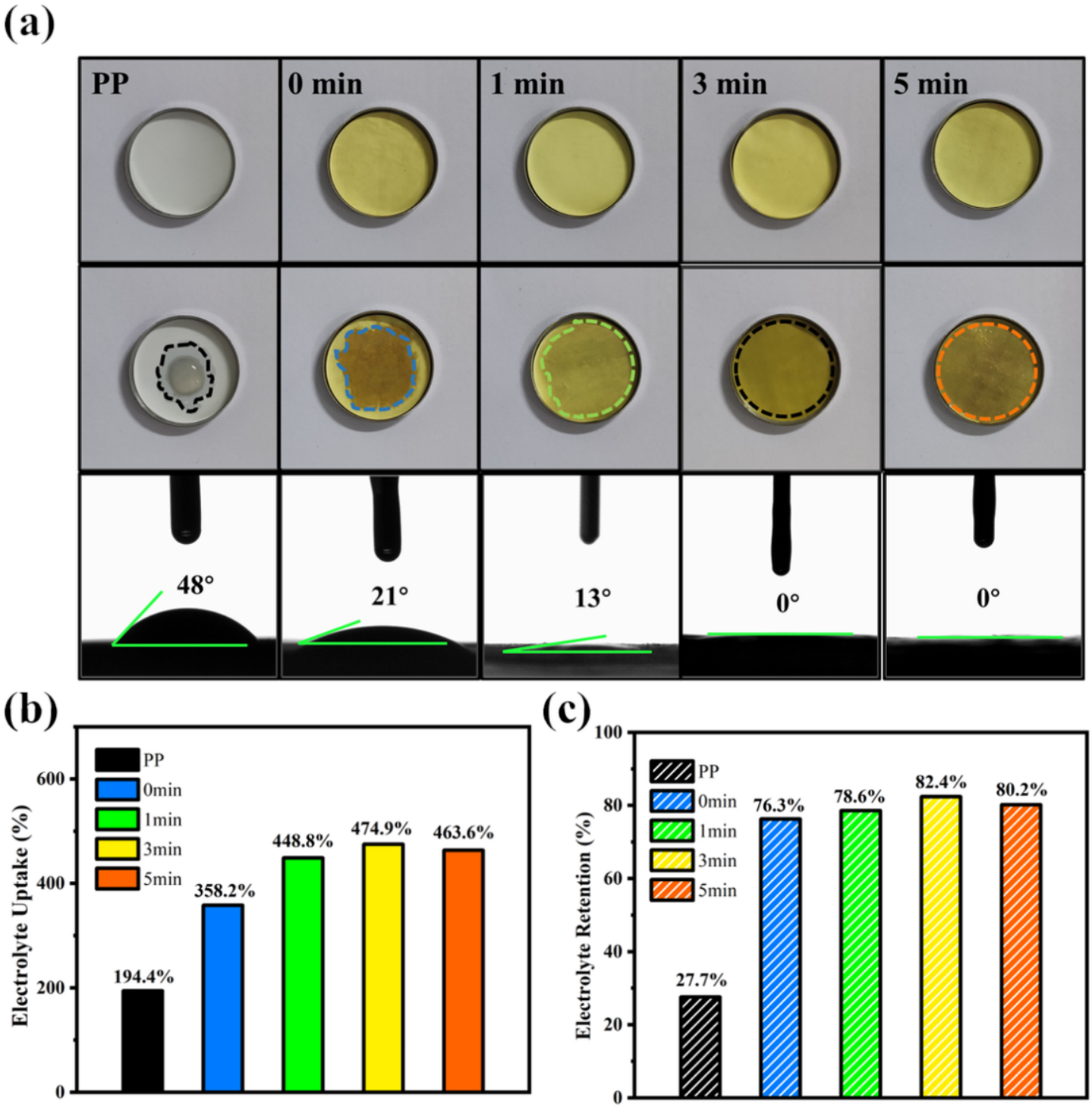

Figure 8

(a) Electrolyte droplet addition and contact angle; (b) Electrolyte absorption rate; (c) Electrolyte retention rate of PP separator and PI/PAN@CA/PI separator after alkali etching for 0, 1, 3, and 5 min

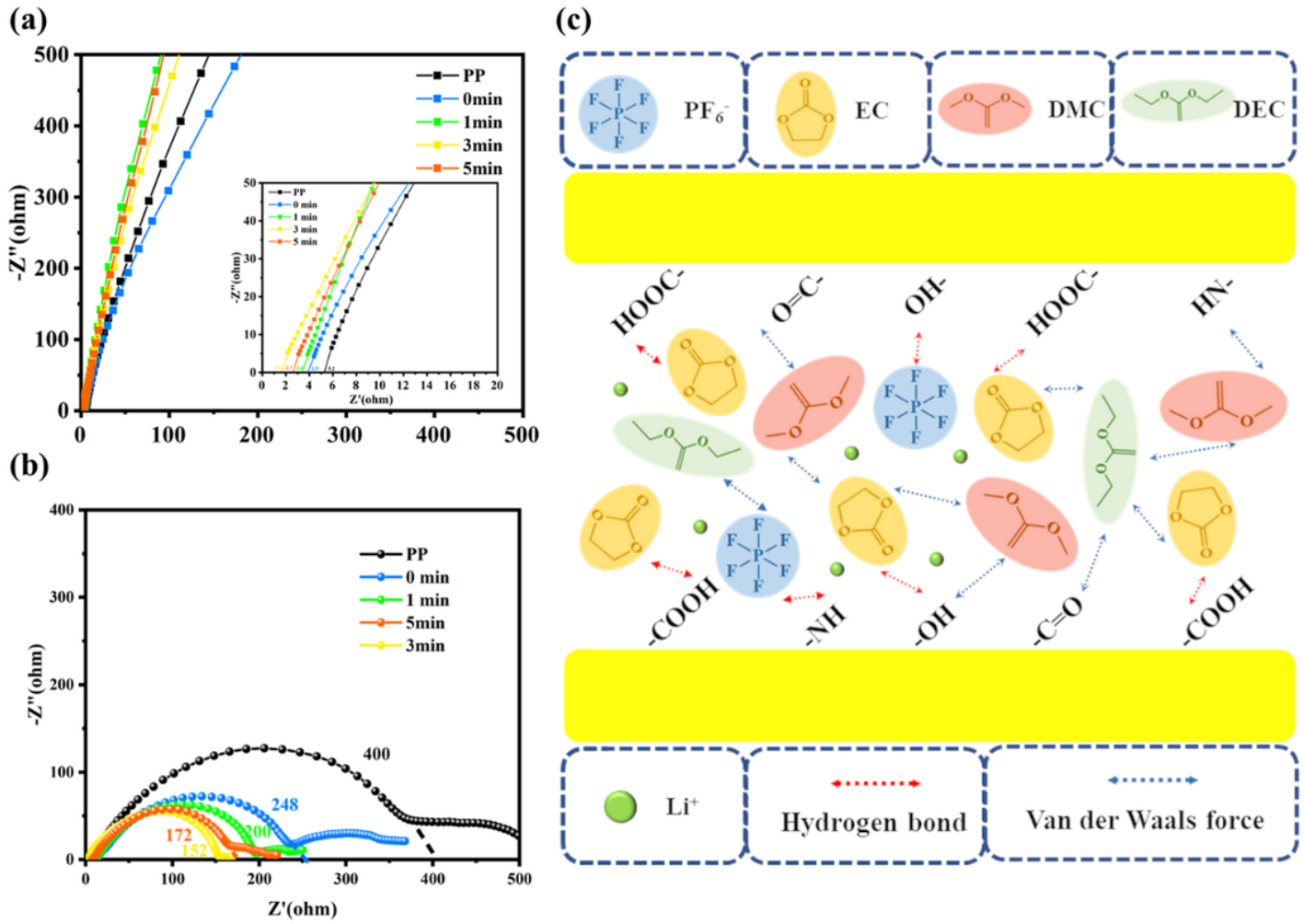

Figure 9

The Nyquist plots of (a) “SS/Separator/SS” cells and (b) “Li/Separator/Li” cells using PP separator and PI/PAN@CA/PI separator after alkali etching for 0, 1, 3, and 5 min; (c) Mechanism diagram of the interaction between polar groups and electrolytes.

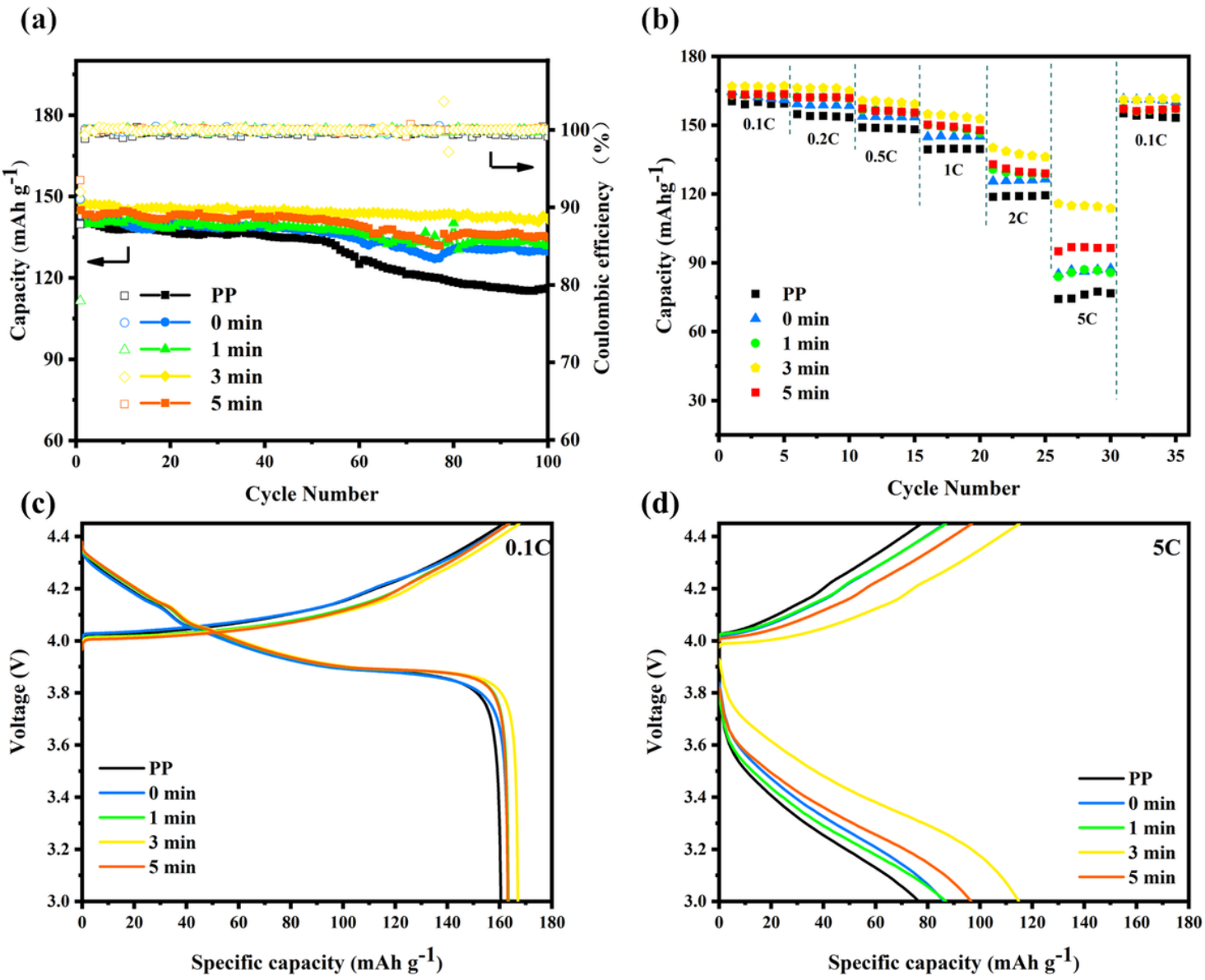

Figure 10

The "$LiCoO_2$/separator/Li" battery using PP separator and PI/PAN@CA/PI separator after 0, 1, 3, and 5 min of alkali etching (a) cyclic testing and Coulombic efficiency at 1 C, (b) discharge specific capacity at different magnification, (c) charge discharge curve of 0.1 C, (d) charge discharge curve of 5 C.